LETTER

doi:10.1038/nature13168

Listeria monocytogenes exploits efferocytosis to promote cell-to-cell spread

Mark A. Czuczman[1,2], Ramzi Fattouh[1], Jorik M. van Rijn[3], Veronica Canadien[1], Suzanne Osborne[1], Aleixo M. Muise[1,4,5,6], Vijay K. Kuchroo[7], Darren E. Higgins[8] & John H. Brumell[1,2,5,6]

Efferocytosis, the process by which dying or dead cells are removed by phagocytosis, has an important role in development, tissue homeostasis and innate immunity[1]. Efferocytosis is mediated, in part, by receptors that bind to exofacial phosphatidylserine (PS) on cells or cellular debris after loss of plasma membrane asymmetry. Here we show that a bacterial pathogen, *Listeria monocytogenes*, can exploit efferocytosis to promote cell-to-cell spread during infection. These bacteria can escape the phagosome in host cells by using the pore-forming toxin listeriolysin O (LLO) and two phospholipase C enzymes[2]. Expression of the cell surface protein ActA allows *L. monocytogenes* to activate host actin regulatory factors and undergo actin-based motility in the cytosol, eventually leading to formation of actin-rich protrusions at the cell surface. Here we show that protrusion formation is associated with plasma membrane damage due to LLO's pore-forming activity. LLO also promotes the release of bacteria-containing protrusions from the host cell, generating membrane-derived vesicles with exofacial PS. The PS-binding receptor TIM-4 (encoded by the *Timd4* gene) contributes to efficient cell-to-cell spread by *L. monocytogenes* in macrophages *in vitro* and growth of these bacteria is impaired in *Timd4*$^{-/-}$ mice. Thus, *L. monocytogenes* promotes its dissemination in a host by exploiting efferocytosis. Our results indicate that PS-targeted therapeutics may be useful in the fight against infections by *L. monocytogenes* and other bacteria that use similar strategies of cell-to-cell spread during infection.

The intermediate stages of cell-to-cell spread by *L. monocytogenes* remain unclear. On the basis of observations with an *in vitro* infection model, it has been suggested that bacteria-containing protrusions are released from infected cells before uptake of membrane vesicles containing bacteria by neighbouring cells[3]. However, the mechanisms that mediate protrusion release and uptake of bacteria in vesicles are not known.

LLO is required for *L. monocytogenes* cell-to-cell spread in some cell types, including macrophages[4,5]. LLO is a pore-forming toxin that is often referred to as a 'phagosome-specific lysin'[6] because it has limited activity in the cytosol of host cells, owing to its relatively low lytic activity[7] and stability[8] at neutral pH. Furthermore, LLO is degraded by the proteasome[9]. Despite these factors, it is now appreciated that LLO can damage the plasma membrane of host cells[10]. Host membrane repair pathways limit LLO-mediated membrane damage[11], but the mechanisms by which they act remain unclear. LLO is essential for disruption of the outer membrane of spreading vacuoles[4]. Whether LLO contributes to other stages of cell-to-cell spread has not been tested.

We proposed that LLO-mediated damage to the plasma membrane may promote cell-to-cell spread. We used a propidium iodide (PI) assay to measure membrane damage induced during *L. monocytogenes* infection (Fig. 1a). Repair of the plasma membrane is a Ca^{2+}-dependent process[12]. Therefore, the absence of Ca^{2+} in the medium provided a convenient method to inactivate endogenous repair mechanisms and visualize the full extent of membrane damage. HeLa cells were used for these studies as phagosome escape by *L. monocytogenes* does not require LLO in this cell type[13].

In the absence of extracellular Ca^{2+}, infection of cells with wild-type bacteria revealed an increase in membrane damage compared with uninfected cells (Fig. 1b, c). The number of PI^+ cells increased over time, indicating that membrane damage was an ongoing event during infection. Less damage was observed when Ca^{2+} was present in the extracellular medium, suggesting that Ca^{2+}-dependent repair pathways limit plasma membrane damage.

Caspase 7 promotes membrane repair during *L. monocytogenes* infection of macrophages[11]. Consistent with this, we found that short interfering RNA (siRNA)-mediated knockdown of caspase 7 increased membrane damage induced by *L. monocytogenes* (Extended Data Fig. 1a, b). However, this effect was minor, indicating that other factors contribute to membrane repair. Annexins also have a role in membrane repair[14]. We found that siRNA-mediated knockdown of annexins A1, A2 and A6 led to an increase in membrane damage (Extended Data Fig. 1a, b). We conclude that multiple host factors contribute to repair of the plasma membrane during *L. monocytogenes* infection.

LLO damages host membranes during infection[10,11]. Consistent with this, a mutant lacking LLO (Δ*hly*) was impaired in membrane damage, and complementation with *hly* restored membrane damage (Fig. 1d and Extended Data Fig. 2a). Deletion of both phospholipase C (PLC) enzymes had no effect on membrane damage in Ca^{2+}-free media. However, PLCs were required for membrane damage in Ca^{2+}-containing media, suggesting that they may promote LLO activity and/or inhibit membrane repair mechanisms. We observed a decrease in membrane damage in cells infected with ActA-deficient (Δ*actA*) bacteria. Treatment of cells with the actin inhibitors latrunculin B or cytochalasin D had a similar effect (Extended Data Fig. 2b). Thus, actin-based motility may promote membrane damage by LLO by allowing close apposition of bacteria to the plasma membrane.

Membrane damage is associated with the loss of membrane asymmetry and redistribution of PS to the outer leaflet of the plasma membrane[15]. Therefore, to visualize membrane damage induced by *L. monocytogenes* we stained cells with a probe (annexin A5–Alexa 488) to label exofacial PS. In uninfected cells, low amounts of exofacial PS were detected (Extended Data Fig. 3). By contrast, treatment of cells with saponin led to staining of cells with annexin A5–Alexa 488.

In cells infected by wild-type bacteria, we observed the formation of PS^+ structures at the cell surface (Fig. 2a, right, and Extended Data Fig. 4). These structures co-localized with bacteria (visualized by red fluorescent protein (RFP) expression[16]) and were not associated with cellular blebbing, rounding or nuclear condensation, indicating that they were not the consequence of apoptosis. Extracellular bacteria did not label with annexin A5–Alexa 488 and bacteria present in PS^+ structures were not accessible to anti-*L. monocytogenes* antibodies (Extended Data Fig. 5). This indicated that PS^+ bacteria were present in a host-derived membrane

[1]Cell Biology Program, Hospital for Sick Children, Toronto, Ontario M5G0A4, Canada. [2]Department of Molecular Genetics, University of Toronto, Toronto, Ontario M5S1A8, Canada. [3]Department of Cell Biology and Institute of Biomembranes, University Medical Center Utrecht, 3584 CX Utrecht, the Netherlands. [4]Division of Gastroenterology, Hepatology, and Nutrition, Department of Paediatrics, Hospital for Sick Children, Toronto, Ontario M5G1X8, Canada. [5]Institute of Medical Science, University of Toronto, Toronto, Ontario M5S1A8, Canada. [6]Sickkids IBD Centre, Hospital for Sick Children, Toronto, Ontario M5G1X8, Canada. [7]Center for Neurologic Diseases, Brigham and Women's Hospital, Harvard Medical School, Boston, Massachusetts 02115, USA. [8]Department of Microbiology and Immunobiology, Harvard Medical School, Boston, Massachusetts 02115, USA.

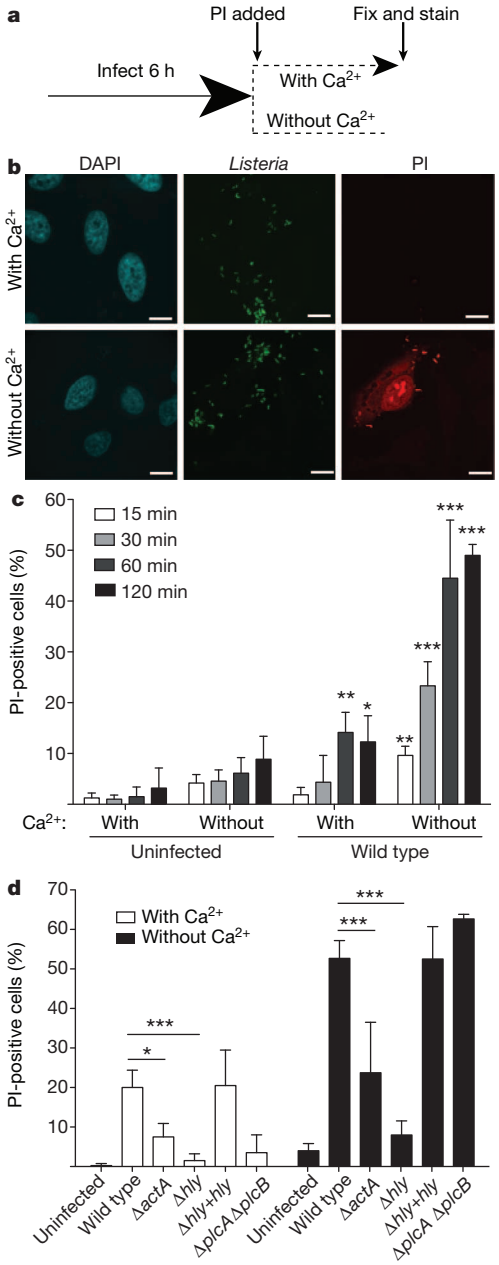

Figure 1 | Actin-based motility promotes LLO-mediated membrane damage. **a**, Experimental design for membrane damage assay. **b**, Confocal images of HeLa cells infected as in **a** with wild-type *L. monocytogenes* at a multiplicity of infection (MOI) of 100. DAPI, 4′,6-diamidino-2-phenylindole. Scale bars, 10 μm. Images are representative of three independent experiments. **c**, Cells were infected as in **a** for the indicated time and PI^+ cells were enumerated ($n = 100$). Data are shown as averages ± standard deviation (s.d.) for four independent experiments. *P* values were calculated using two-tailed Student's *t*-test. **d**, Averages ± s.d. for three independent experiments are shown. *P* values were calculated using one-way analysis of variance (ANOVA). $*P < 0.05$, $**P < 0.01$, $***P < 0.001$.

structure. Correlative microscopy revealed that the PS^+ structures were associated with the surface of infected cells (Fig. 2a, left). Formation of PS^+ structures required LLO, consistent with a role for membrane damage in their formation (Fig. 2b, c). PS^+ structures were also observed in Henle-407 cells and murine bone-marrow-derived macrophages (BMDMs) (Extended Data Fig. 6).

Several lines of evidence indicated that PS^+ structures are associated with protrusion formation. First, we observed filamentous PS^+ structures connected to bacteria that resembled protrusions (Fig. 2b, top).

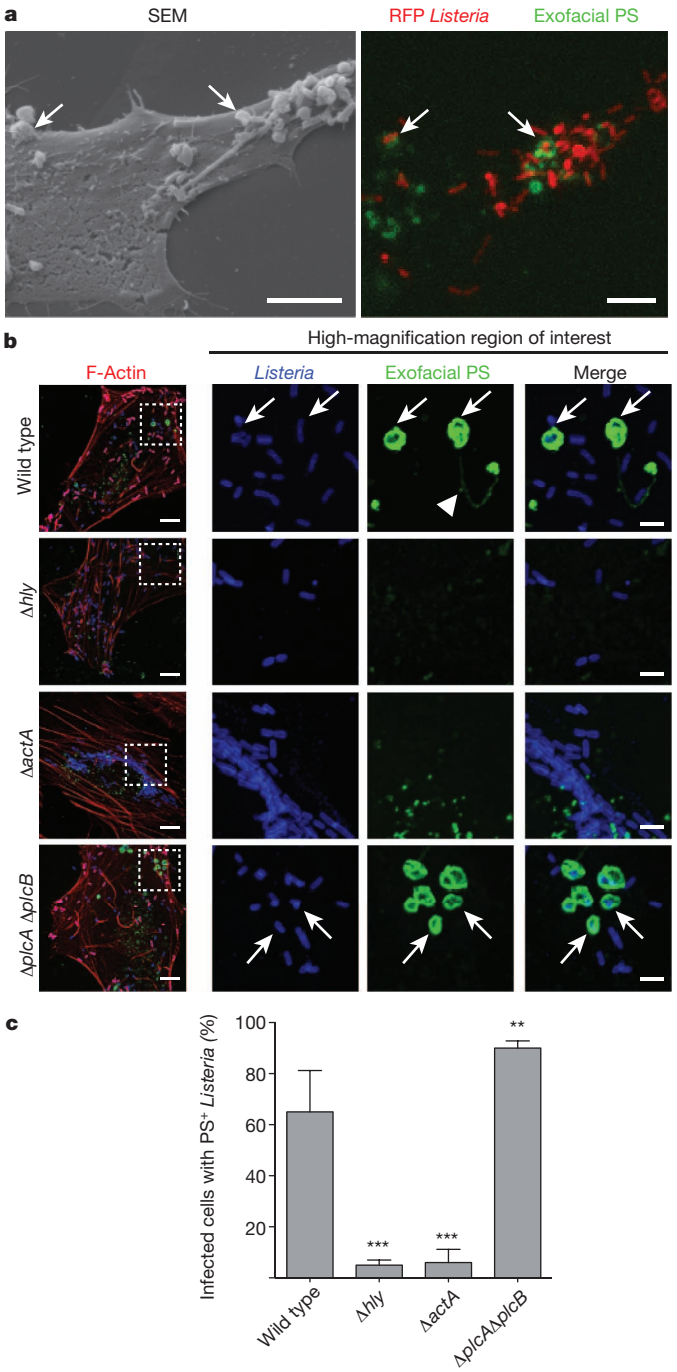

Figure 2 | Formation of PS^+ structures during *L. monocytogenes* infection. **a**, HeLa cells were infected at an MOI of 100 with wild-type *L. monocytogenes* expressing RFP (red) for 6 h and then incubated with a probe for exofacial PS (annexin A5–Alexa 488; green). Cells were then fixed and analysed by fluorescence microscopy to identify PS^+ structures and *L. monocytogenes* (right). Scanning electron microscopy (SEM) of the same cell shows PS^+ structures (left). Images are representative of two independent experiments. Scale bars, 5 μm. **b**, Confocal images of cells infected with the indicated strain for 6 h. Boxed areas (left) are low-magnification images (a three-colour merge, includes phalloidin stain for F-actin); they are enlarged on the right. Arrows indicate *L. monocytogenes* bacteria that co-localize with PS, and arrowhead indicates PS^+ filaments. Images are representative of three independent experiments. Scale bars, 10 μm for low-magnification merge, and 3 μm for enlarged panels. **c**, Cells containing PS^+ bacteria enumerated for **b**. Averages ± s.d. for three independent experiments are shown ($n = 100$). *P* values were calculated using one-way ANOVA. $**P < 0.01$, $***P < 0.001$.

Second, Δ*actA* mutants did not form these structures (Fig. 2b, c). Third, we observed that the kinetics of formation of PS^+ structures were similar to the kinetics of protrusion formation (marked by ezrin[17]; Fig. 3a). Live cell imaging revealed that bacteria-containing protrusions (marked by LifeAct–RFP) rapidly recruited the exofacial PS probe, before rounding of the PS^+ protrusion into vesicles on the cell surface (Fig. 3b and Supplementary Video 1). Recruitment of the exofacial PS probe was limited to protrusions and vesicles, indicating that loss of membrane asymmetry was not the result of global cellular membrane damage. Annexin A2 was localized to PS^+ bacteria (Extended Data Fig. 1c), suggesting that membrane repair pathways serve to locally restrict membrane damage.

Streptolysin O, a pore-forming toxin from group A *Streptococcus*, has been shown to induce membrane blebbing and release of plasma-membrane-derived vesicles[18,19]. Our studies indicated that *L. monocytogenes* similarly induces the release of membrane vesicles through LLO. PS^+ structures containing bacteria were observed on coverslips with no connections to infected cells (Extended Data Fig. 7a). We also isolated these vesicles by centrifugation of the medium (Extended Data Fig. 7b). Our findings suggest that bacteria-containing protrusions are released by infected host cells, giving rise to PS^+ vesicles in the medium and that, in some cases, these vesicles remain associated with the cell surface of infected cells. Deletion of both PLCs caused an increase in the number of PS^+ structures associated with the surface of infected cells (Fig. 2b, c). Thus, PLCs may promote bacterial escape from PS^+ structures after their release from infected cells, which would be consistent with the role of PLCs in escape from vacuoles in secondarily infected cells[4].

Efferocytosis receptors mediate uptake of PS^+ cells and cellular debris[1]. In macrophages, TIM-4 has a key role in efferocytosis[20,21]. Because macrophages are a major target of *L. monocytogenes* during systemic infection, we examined the role of TIM-4 in cell-to-cell spread by these bacteria using an infection focus assay. The foci of infection in BMDMs from *Timd4*$^{-/-}$ mice contained fewer infected cells compared with control BMDMs from C57BL/6 mice (Fig. 4a, b). Using live cell imaging, we observed that infection foci were smaller in BMDM cultures from *Timd4*$^{-/-}$ mice from 8 to 18 h post-infection (Fig. 4c, d). Bacterial replication within primarily infected *Timd4*$^{-/-}$ BMDMs at low cell density (minimizing cell-to-cell spread) was comparable with that of control BMDMs (Extended Data Fig. 8). This indicated that deficient bacterial spread in *Timd4*$^{-/-}$ BMDM cultures was not due to impaired bacterial replication in the cytosol of these cells. Blocking antibodies that targeted either TIM-4 or PS impaired bacterial spread in cultures of control but not *Timd4*$^{-/-}$ BMDMs (Fig. 4b), indicating that TIM-4 promotes bacterial cell-to-cell spread through its ability to bind PS^+ structures.

TIM-4 was previously shown to suppress pro-inflammatory cytokine production *in vivo*[22]. Therefore, we considered the possibility that TIM-4 deficiency impairs cell-to-cell spread by *L. monocytogenes* indirectly, through enhanced pro-inflammatory cytokine production. However, in our *in vitro* experiments, pro-inflammatory cytokine production was typically not observed until 18 h post-infection (after bacterial spread is initiated) and shared the same profile of expression in both control and *Timd4*$^{-/-}$ BMDM cultures (Extended Data Fig. 9a). This suggested that TIM-4 acts in a cell-autonomous manner to promote cell-to-cell spread by *L. monocytogenes*.

To test this hypothesis, we used a cell-to-cell spread assay that measures the direct transmission of bacteria from primary infected cells to secondary cells (labelled with CellTrackerBlue). Primary cells were infected with a bacterial mutant lacking both PLCs (Δ*plcA*Δ*plcB*), as this prevents bacterial escape from spreading vacuoles and avoids the confounding effect of rapid replication in the cytosol of secondary cells. Bacterial spread to secondary BMDMs from *Timd4*$^{-/-}$ mice was reduced compared with control mice (Fig. 4e). Microscopic analysis revealed higher numbers of $actin^+$ protrusions associated with secondary BMDMs from control mice compared with *Timd4*$^{-/-}$ mice (Fig. 4f, g). This suggests that TIM-4 may promote the association and/or stability of protrusions as they project from infected cells into adjacent cells. Together, our findings indicate a specific role for TIM-4 in mediating cell-to-cell spread by *L. monocytogenes*.

We observed decreased numbers of bacteria in the liver and spleen of *Timd4*$^{-/-}$ mice compared with control mice (Fig. 4h). Similar numbers of Δ*actA* mutant bacteria were observed in the liver of control and *Timd4*$^{-/-}$ mice (Fig. 4i), indicating that TIM-4 is required for pathogenesis of motile bacteria in this organ and consistent with its role in promoting bacterial cell-to-cell spread. However, we observed a decrease in survival of Δ*actA* mutant bacteria in spleens of infected *Timd4*$^{-/-}$ mice. We also observed elevated basal levels of pro-inflammatory cytokines in the spleens (and to a lesser extent the livers) of *Timd4*$^{-/-}$ mice before infection (Extended Data Fig. 9b). Together, our findings suggest that *L. monocytogenes* exploits TIM-4 during systemic infection of mice by two mechanisms; directly, through uptake of PS^+ bacteria, and indirectly, through the ability of TIM-4 to suppress pro-inflammatory cytokine production.

It has previously been demonstrated that TIM-4 mediates the clearance of apoptotic macrophages bearing *Mycobacterium tuberculosis*[23].

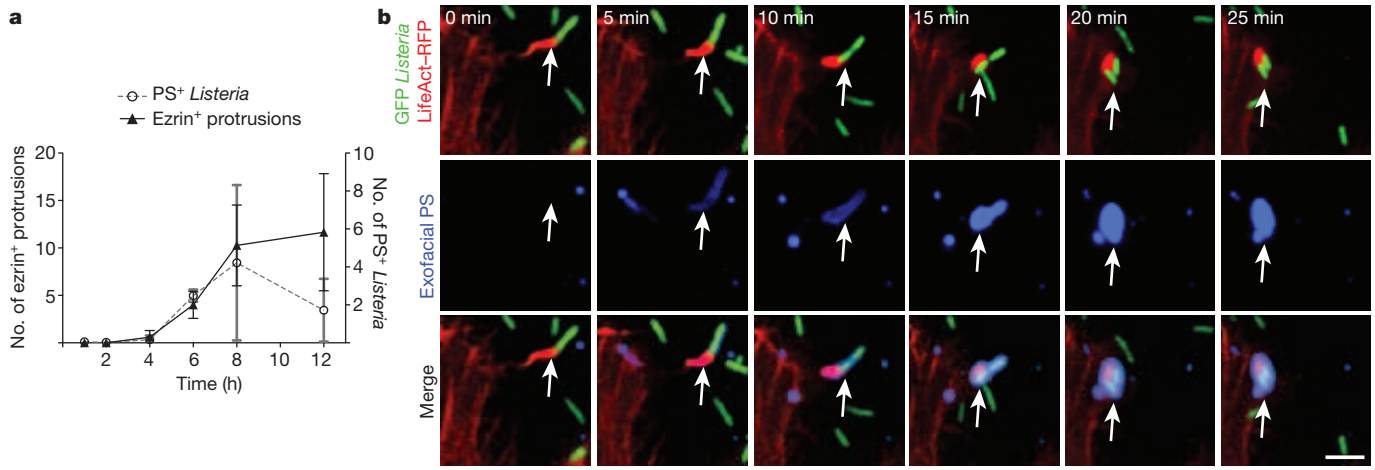

Figure 3 | Protrusions give rise to PS^+ vesicles containing *L. monocytogenes*. **a**, PS^+ bacteria and $ezrin^+$ protrusions were enumerated in HeLa cells infected at an MOI of 100 with wild-type *L. monocytogenes* for the indicated time. Averages ± s.d. for three independent experiments are shown ($n = 100$). **b**, Cells were transfected with LifeAct–RFP (F-actin probe) and then infected with wild-type *L. monocytogenes* expressing GFP for 6 h. Live infected cells were analysed by spinning-disk confocal microscopy with annexin A5–Alexa 647 in the medium to label exofacial PS (green). Successive frames are shown. Arrows indicates protrusion that acquires PS. Images are representative of four independent experiments. Scale bar, 10 μm.

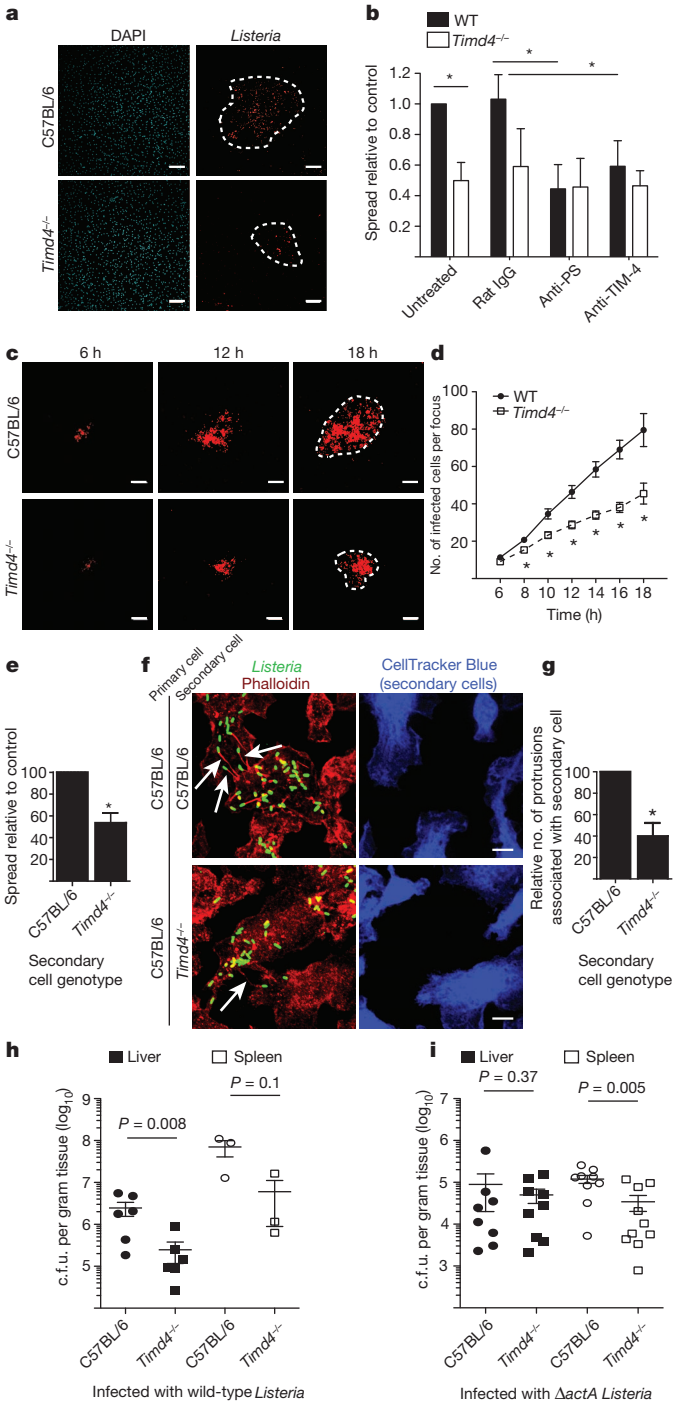

Figure 4 | TIM-4 promotes *L. monocytogenes* cell-to-cell spread in macrophages and growth in mice. **a**, Infection focus assay for measuring cell-to-cell spread. BMDMs were infected with *L. monocytogenes* at an MOI of 0.01. Images are representative of three independent experiments. Dotted lines delineate infection foci. Scale bars, 100 μm. **b**, Infection foci from **a** were enumerated by fluorescence microscopy. A total of 100 infection foci were analysed for each genotype/strain. Where indicated, cells were treated with anti-PS, anti-TIM-4 or non-specific rat IgG (control) during infection. WT, wild type. Averages ± s.d. for three independent experiments are shown. *P* values were calculated using two-way ANOVA with Bonferroni post-test. **c**, Monolayers of control or *Timd4*$^{-/-}$ BMDMs were infected at an MOI of 0.01 with *L. monocytogenes* expressing RFP and examined by live cell imaging. Images are representative of two independent experiments. Dotted lines delineate infection foci. Scale bars, 100 μm. **d**, The number of infected cells per focus from **c**. Averages ± s.d. for two independent experiments are shown ($n = 10$). *P* values were calculated using two-tailed Student's *t*-test. **e**, Cell-to-cell spread assay. Averages ± s.d. for three independent experiments are shown ($n = 100$). *P* values were calculated using two-tailed Student's *t*-test. **f**, Images from **e**. Arrows indicate actin^{+} protrusions associated with secondary cells. Images are representative of four independent experiments ($n = 100$). Scale bars, 10 μm. **g**, Actin^{+} protrusions associated with secondary cells were enumerated. Averages ± s.d. for four independent experiments are shown. **h**, **i**, Mice were infected with 5×10^4 colony-forming units (c.f.u.) wild-type (**h**) or 1×10^7 c.f.u. Δ*actA* mutant (**i**) *L. monocytogenes* by tail vein injection. Mice were killed and livers and spleen were harvested at 72 h after infection for quantification of bacterial load (c.f.u. per gram tissue). Data are expressed as mean ± standard error of the mean. *P* values were calculated using one-tailed Mann–Whitney test.

This finding indicates an important role for efferocytosis in innate immunity. By contrast, our findings suggest that efferocytosis can be exploited by *L. monocytogenes* to promote cell-to-cell spread. Other mechanisms also contribute to *L. monocytogenes* dissemination in a host[24–26]. Viruses are known to exploit efferocytosis by incorporating PS into their viral membrane[27,28]. *L. monocytogenes* does not incorporate PS into its cellular wall but rather exploits host membrane repair mechanisms to promote release of protrusion-associated membrane, giving rise to a PS^{+} 'cloak' that can promote efferocytosis (see model in Extended Data Fig. 10). Similar forms of non-lytic ejection of bacteria from host cells have been described for *Mycobacterium marinum*[29] and *Chlamydia trachomatis*[30], indicating that these (and probably other) pathogens may also exploit efferocytosis during infection. In summary, our study identifies a novel strategy used by pathogenic bacteria to promote their dissemination in a host and provides a remarkable example of how pathogens can exploit innate immune defences during infection.

METHODS SUMMARY

All *L. monocytogenes* strains were derivatives of 10403S and are listed in Methods. Six-to-eight-week-old C57BL/6 and *Timd4*$^{-/-}$ mice were used to generate BMDMs or were infected intravenously for systemic infection studies. Cytokine levels were measured using a mouse 7-plex pro-inflammatory kit. *In vitro* infections of confluent cell monolayers were performed at an MOI of 0.1–100, as indicated in figure legends, and were performed in the presence of gentamicin to prevent extracellular growth. Constructs, antibodies, siRNA and other pharmacological reagents are listed in Methods. PI staining was carried out 6 h post-infection in Tyrode's buffer in the presence or absence of calcium. Annexin A5–Alexa 488 was added to chilled cells for exofacial PS staining. Staining protocols are indicated in Methods. For the infection focus assay, confluent monolayers of BMDMs were infected for 18 h and the size of infection foci was analysed. For the direct cell-to-cell spread assay, primary cells were lifted with CellStripper and overlaid onto fresh cultures of CellTrackerBlue-labelled cells for 90 min.

Unless indicated, cells were fixed with paraformaldehyde. Quantifications were done on a Leica DMIRE2 epifluorescence microscope with ×63 objective. Correlative electron microscopy images were acquired from dehydrated samples gold coated in a Denton Desk II sputter coater and examined under a FEI XL30 SEM. Confocal z stacks (2 μm) were taken with a Quorum spinning disk microscope, analysed with Volocity 6 software and imported into Adobe Illustrator. Nikon Ti-E microscopy was used to acquire images of infection foci at ×10 magnification.

The mean plus s.d. is shown in figures. *P* values were calculated using GraphPad Prism v.4.0a using statistical tests indicated in figure legends. A *P* value less than 0.05 was considered significant.

Online Content Any additional Methods, Extended Data display items and Source Data are available in the online version of the paper; references unique to these sections appear only in the online paper.

Received 22 February 2013; accepted 21 February 2014.
Published online 13 April 2014.

1. Ravichandran, K. S. Beginnings of a good apoptotic meal: the find-me and eat-me signaling pathways. *Immunity* **35,** 445–455 (2011).
2. Mostowy, S. & Cossart, P. Virulence factors that modulate the cell biology of *Listeria* infection and the host response. *Adv. Immunol.* **113,** 19–32 (2012).
3. Robbins, J. R. *et al. Listeria monocytogenes* exploits normal host cell processes to spread from cell to cell. *J. Cell Biol.* **146,** 1333–1350 (1999).
4. Alberti-Segui, C., Goeden, K. R. & Higgins, D. E. Differential function of *Listeria monocytogenes* listeriolysin O and phospholipases C in vacuolar dissolution following cell-to-cell spread. *Cell. Microbiol.* **9,** 179–195 (2007).

5. Gedde, M. M., Higgins, D. E., Tilney, L. G. & Portnoy, D. A. Role of listeriolysin O in cell-to-cell spread of *Listeria monocytogenes*. *Infect. Immun.* **68,** 999–1003 (2000).
6. Schnupf, P. & Portnoy, D. A. Listeriolysin O: a phagosome-specific lysin. *Microbes Infect.* **9,** 1176–1187 (2007).
7. Glomski, I. J., Gedde, M. M., Tsang, A. W., Swanson, J. A. & Portnoy, D. A. The *Listeria monocytogenes* hemolysin has an acidic pH optimum to compartmentalize activity and prevent damage to infected host cells. *J. Cell Biol.* **156,** 1029–1038 (2002).
8. Nomura, T. *et al.* Irreversible loss of membrane-binding activity of *Listeria*-derived cytolysins in non-acidic conditions: a distinct difference from allied cytolysins produced by other Gram-positive bacteria. *Microbiology* **153,** 2250–2258 (2007).
9. Schnupf, P., Portnoy, D. A. & Decatur, A. L. Phosphorylation, ubiquitination and degradation of listeriolysin O in mammalian cells: role of the PEST-like sequence. *Cell. Microbiol.* **8,** 353–364 (2006).
10. Hamon, M. A., Ribet, D., Stavru, F. & Cossart, P. Listeriolysin O: the Swiss army knife of *Listeria*. *Trends Microbiol.* **20,** 360–368 (2012).
11. Cassidy, S. K. *et al*. Membrane damage during *Listeria monocytogenes* infection triggers a caspase-7 dependent cytoprotective response. *PLoS Pathog.* **8,** e1002628 (2012).
12. Idone, V., Tam, C. & Andrews, N. W. Two-way traffic on the road to plasma membrane repair. *Trends Cell Biol.* **18,** 552–559 (2008).
13. Gründling, A., Gonzalez, M. D. & Higgins, D. E. Requirement of the *Listeria monocytogenes* broad-range phospholipase PC-PLC during infection of human epithelial cells. *J. Bacteriol.* **185,** 6295–6307 (2003).
14. Draeger, A., Monastyrskaya, K. & Babiychuk, E. B. Plasma membrane repair and cellular damage control: the annexin survival kit. *Biochem. Pharmacol.* **81,** 703–712 (2011).
15. Fadeel, B. & Xue, D. The ins and outs of phospholipid asymmetry in the plasma membrane: roles in health and disease. *Crit. Rev. Biochem. Mol. Biol.* **44,** 264–277 (2009).
16. Waite, J. C. *et al.* Dynamic imaging of the effector immune response to *Listeria* infection *in vivo*. *PLoS Pathog.* **7,** e1001326 (2011).
17. Pust, S., Morrison, H., Wehland, J., Sechi, A. S. & Herrlich, P. *Listeria monocytogenes* exploits ERM protein functions to efficiently spread from cell to cell. *EMBO J.* **24,** 1287–1300 (2005).
18. Babiychuk, E. B., Monastyrskaya, K., Potez, S. & Draeger, A. Blebbing confers resistance against cell lysis. *Cell Death Differ.* **18,** 80–89 (2011).
19. Keyel, P. A. *et al.* Streptolysin O clearance through sequestration into blebs that bud passively from the plasma membrane. *J. Cell Sci.* **124,** 2414–2423 (2011).
20. Feng, D. *et al.* Cellular internalization of exosomes occurs through phagocytosis. *Traffic* **11,** 675–687 (2010).
21. Miyanishi, M. *et al.* Identification of Tim4 as a phosphatidylserine receptor. *Nature* **450,** 435–439 (2007).
22. Rodriguez-Manzanet, R. *et al.* T and B cell hyperactivity and autoimmunity associated with niche-specific defects in apoptotic body clearance in TIM-4-deficient mice. *Proc. Natl Acad. Sci. USA* **107,** 8706–8711 (2010).
23. Martin, C. J. *et al.* Efferocytosis is an innate antibacterial mechanism. *Cell Host Microbe* **12,** 289–300 (2012).
24. Appelberg, R. & Leal, I. S. Mutants of *Listeria monocytogenes* defective in *in vitro* invasion and cell-to-cell spreading still invade and proliferate in hepatocytes of neutropenic mice. *Infect. Immun.* **68,** 912–914 (2000).
25. Drevets, D. A. Dissemination of *Listeria monocytogenes* by infected phagocytes. *Infect. Immun.* **67,** 3512–3517 (1999).
26. Friedrich, N., Hagedorn, M., Soldati-Favre, D. & Soldati, T. Prison break: pathogens' strategies to egress from host cells. *Microbiol. Mol. Biol. Rev.* **76,** 707–720 (2012).
27. Meertens, L. *et al.* The TIM and TAM families of phosphatidylserine receptors mediate dengue virus entry. *Cell Host Microbe* **12,** 544–557 (2012).
28. Mercer, J. & Helenius, A. Vaccinia virus uses macropinocytosis and apoptotic mimicry to enter host cells. *Science* **320,** 531–535 (2008).
29. Hagedorn, M., Rohde, K. H., Russell, D. G. & Soldati, T. Infection by tubercular mycobacteria is spread by nonlytic ejection from their amoeba hosts. *Science* **323,** 1729–1733 (2009).
30. Hybiske, K. & Stephens, R. S. Mechanisms of host cell exit by the intracellular bacterium *Chlamydia*. *Proc. Natl Acad. Sci. USA* **104,** 11430–11435 (2007).

Supplementary Information is available in the online version of the paper.

Acknowledgements We are grateful to S. Gray-Owen, S. Grinstein and D. Portnoy for providing reagents and advice and to D. Holmyard for help with electron microscopy. J.H.B. holds the Pitblado Chair in Cell Biology. Infrastructure for the Brumell laboratory was provided by a Leader's Opportunity Fund grant from the Canadian Foundation for Innovation and the Ontario Innovation Trust. R.F. was supported by a postdoctoral fellowship from the Canadian Institutes of Health Research in partnership with the Canadian Association of Gastroenterology and the Crohn's and Colitis Foundation of Canada. S.O. was supported by a postdoctoral fellowship from the Research Training Committee at the Hospital for Sick Children. This work was supported by an operating grant from The Arthritis Society of Canada (#RG11/013) to J.H.B. and a US Public Health Service grant (AI053669) from the National Institutes of Health to D.E.H.

Author Contributions J.H.B., M.A.C., S.O. and D.E.H. designed the experiments and wrote the paper. M.A.C., R.F., J.M.v.R., V.C. and S.O. performed the experiments. A.M.M. and V.K.K. contributed reagents and consultations.

Author Information Reprints and permissions information is available at www.nature.com/reprints. The authors declare no competing financial interests. Readers are welcome to comment on the online version of the paper. Correspondence and requests for materials should be addressed to J.H.B. (john.brumell@sickkids.ca).

METHODS

Bacterial strains. *L. monocytogenes* were grown in brain-heart infusion (BHI) broth and the following strains were used: 10403S (wild type)[31], DP-L2161 (Δ*hly*)[32], DP-L4818 (Δ*hly* + *hly*)[33], DP-L3078 (Δ*actA*)[34], and DP-L1936 (Δ*plcA* Δ*plcB*)[35]. Wild-type *L. monocytogenes* 10403S expressing TagRFP under the *actA* promoter (DP-L5538)[16] or expressing GFP under the *hly* promoter (DP-L1039) were previously described[36].

Antibodies, constructs and reagents. Primary antibodies used were rabbit anti-annexin A2 (#610068 from BD Biosciences), rabbit anti-GFP (#A11120 from Invitrogen), rabbit anti-caspase 7 (#12827 from Cell Signaling), rabbit anti-*Listeria* (#B223021 from BD Biosciences), rabbit anti-*L. monocytogenes* antibody (gift from P. Cossart), mouse anti-phosphatidylserine (#18005 from Abcam) and mouse anti-ezrin (#35-7300 from Invitrogen). Rat anti-TIM-4 blocking antibody was previously described[37]. Alexa Fluor-568 Phalloidin, annexin A5–Alexa Fluor-488 and -647 conjugates and all fluorescent secondary antibodies (AlexaFluor conjugates) were from Invitrogen. DAPI (#D1306 from Invitrogen) was used at 1:2,500 dilution to stain the nuclei where indicated. Cytochalasin D (#2502555; 10 μM final) and Latrunculin B (#428020; 10 μg ml^{-1} final) were from Calbiochem. For transfection of HeLa cells, Xtreme Gene 9 (Roche) transfection reagent was used as per manufacturer's protocols. LifeAct–mRFP[38] was a gift from R. Truant. The following siRNAs were from Sigma: annexin A1 (#00157996), annexin A2 (#00246294), annexin A6 (#00063383), caspase 7 (#00128361).

Cell culture and macrophage generation. HeLa and Henle-407 cells were cultured in DMEM (Hyclone) supplemented with 10% heat-inactivated FBS (Wisent) without antibiotics at 37 °C and 5% CO_2.

All experimental protocols involving mice were approved by the Animal Care Committee of The Hospital for Sick Children. Mice were euthanized by CO_2 inhalation. Mouse BMDMs were obtained from the dissected femurs and tibias of 5–8-week-old mice. Cells were washed with growth medium and plated on 70 cm^2 Petri dishes. Medium was replaced every 2 days and after 7–9 days cells were used for experiments. Cells were maintained in high-glucose RPMI-1640 medium (Wisent #350-025-CL) containing 10% heat-inactivated FBS (Wisent), 1% sodium pyruvate (Wisent), 1% non-essential amino acids (Wisent), 0.5% 2-mercaptoethanol (Gibco), 1% penicillin and streptomycin (Invitrogen), and 10% L929 medium. L929 medium was generated by growing a confluent layer of L929 cells in 175 cm^2 flasks in DMEM supplemented with 10% heat-inactivated FBS. When cells reached confluency, growth medium was replaced by DMEM alone. After 7 days, supernatant was collected, centrifuged, filtered, and stored at −20 °C.

PI assay for membrane damage. HeLa cells were plated at 5×10^4 cells per well in 24-well tissue culture plates ~18 h before infection. For siRNA treatments, the cells were plated at 2.5×10^4 cells per well. siRNAs were applied after 18 h and the media was changed 24 h later. Infections were carried out 24 h later. All strains of *L. monocytogenes* were infected at an MOI of 100. Bacteria were spun onto cells by centrifugation at 1,500 r.p.m. for 5 min. After 60 min of invasion at 37 °C, cells were washed three times with PBS with calcium and magnesium (PBS+, Wisent #311-420-CL) followed by the addition of growth medium containing 50 μg ml^{-1} gentamicin (Wisent #400-130-IG). At 6 h post-infection, cells were washed two times with PBS without calcium and magnesium (PBS−, Wisent #311-010-CL) and replaced with Tyrode's Buffer (10 mM HEPES, 10 mM glucose, 5 mM potassium chloride, 140 mM sodium chloride, 1 mM EGTA, 1 mM magnesium chloride, 2 mM calcium chloride, pH 7.4) containing 0.5 mg ml^{-1} PI (Sigma #P4170). For Tyrode's Buffer lacking calcium the 2 mM calcium chloride was replaced with 2 mM magnesium chloride. Cells were incubated in Tyrode's Buffer with PI for the indicated times and then fixed with 4% PFA (EM Sciences #15710). Samples were mounted on slides using fluorescence mounting medium (Dako). Quantifications were done using a Leica DMIRE2 epifluorescence microscope equipped with a ×40 objective.

Annexin A5–Alexa 488 staining of exofacial PS. HeLa cells were plated at 5×10^4 cells per well in 24-well tissue culture plates ~18 h before infection. All strains of *L. monocytogenes* were infected at an MOI of 100 in DMEM. Bacteria were spun onto cells by centrifugation at 1,500 r.p.m. for 5 min. After 60 min of invasion at 37 °C, cells were washed three times with PBS+ followed by the addition of growth media containing 50 μg ml^{-1} gentamicin (Wisent #400-130-IG). After indicated times of infection, cells were cooled on ice and washed twice with chilled PBS+. Annexin A5–Alexa Fluor-488 conjugate (Invitrogen) was diluted to 1% (v/v) in chilled PBS with calcium and magnesium and added onto the coverslips for 10 min on ice. Cells were washed twice with chilled PBS+ and fixed with 2.5% paraformaldehyde (PFA) (EM Sciences #15710) for 30 min at 37 °C. Samples were mounted on slides using fluorescence mounting medium (Dako).

Immunofluorescence. Immunostaining was conducted as previously described[39]. Briefly, cells were permeabilized and blocked in PBS containing 0.2% saponin (Calbiochem) and 10% normal goat serum (SS-PBS) for 30 min. Subsequently cells were incubated for 1 h with primary antibodies in SS-PBS. Cells were washed three times with PBS and incubated with secondary Alexa Fluor conjugated antibodies for 1 h. Cells were washed three times with PBS, mounted in fluorescence mounting medium (Dako), and analysed using a Leica DMIRE2 epifluorescence microscope. Confocal pictures were taken using a Quorum spinning disk microscope (Leica DMIRE2 inverted fluorescence microscope equipped with a Hamamatsu back-thinned electron multiplying charge-coupled device camera, spinning disc head, and Volocity 4 software (Improvision)). Confocal images were imported into Adobe Photoshop and assembled in Adobe Illustrator for labelling.

Correlative light-scanning electron microscopy. HeLa cells were plated at 5×10^5 cells per well in 6-well tissue culture plates with etched grid coverslips with imprinted numbers (BELLCO Biotechnology) 24 h before infection. Cells were infected with wild-type *L. monocytogenes* expressing RFP (DP-L5538) at an MOI of 100 in DMEM. Bacteria were spun onto cells by centrifugation at 1,500 r.p.m. for 5 min. After 60 min of invasion at 37 °C, cells were washed three times with PBS+ followed by the addition of growth media containing 50 μg ml^{-1} gentamicin (Wisent #400-130-IG). At 6 h post-infection, cells were cooled on ice and washed twice with chilled PBS+. Annexin A5–Alexa Fluor 488 conjugate (Invitrogen) was diluted to 1% (v/v) in chilled PBS with calcium and magnesium and added onto the coverslips for 10 min on ice. Cells were washed twice with chilled PBS+ and fixed with 2.5% PFA (EM Sciences #15710) for 30 min at 37 °C. Coverslips were imaged by fluorescence microscopy in PBS+. Subsequently, samples were fixed in 2% glutaraldehyde in cacodylate buffer, rinsed in buffer and dehydrated in a graded ethanol series. The samples were critical point dried in a Bal-tec CPD030 critical point dryer, mounted on aluminium stubs, gold coated in a Denton Desk II sputter coater and examined in an FEI XL30 SEM.

Live cell imaging of PS$^+$ structure formation. HeLa cells were plated at 2×10^5 cells per well in 6-well tissue culture plates with glass coverslips 48 h before infection. At 24 h before infection, cells were transfected with LifeAct–RFP. Cells were then infected with wild-type *L. monocytogenes* expressing GFP (DP-L1039) at an MOI of 100 in DMEM. After 60 min of invasion at 37 °C, cells were washed three times with PBS+ followed by the addition of growth media containing 50 μg ml^{-1} gentamicin (Wisent #400-130-IG). At 6 h post-infection, coverslips were washed with PBS+ and transferred into microscope chambers and RPMI-1640 with 10% heat-inactivated FBS (Wisent), 50 μg ml^{-1} gentamicin, 2.5 mM $CaCl_2$ and 2% (v/v) annexin A5–Alexa Fluor 647 conjugate (Invitrogen). HeLa cells were maintained at 37 °C during imaging. A Leica DMIRE2 inverted fluorescence microscope equipped with a Hamamatsu Back-Thinned EM-CCD camera and spinning disk confocal scan head with a ×63 objective and LSM 510 software was used. Volocity software (Improvision) was used to acquire images.

Animals. *Timd4*$^{-/-}$ mice (on a C57BL/6 background) were previously characterized[22] and bred in house at the Hospital for Sick Children Animal Care Facility. C57BL/6 mice, originally from The Jackson Laboratory, were also bred in house and used as controls. All experiments were performed with 7–9-week-old female mice that were maintained on a 12 h light–dark cycle, with food and water available *ad libitum*. Sample size was chosen based on litter size and where possible five mice were used per experiment per group and per bacterial strain. Experiments were not blinded and mice were not randomized. All experiments described in this study were carried out in accordance with the Guide for the Humane Use and Care of Laboratory Animals and were approved by the Hospital for Sick Children's Animal Care Committee.

Infection focus assay. After 7–10 days of differentiation, BMDMs were washed twice and detached with ice-cold Versene buffer (0.8 mM EDTA, 1 mM glucose in PBS−) for 20 min at 4 °C. BMDMs were then seeded onto coverslips in 24-well tissue culture plates at 8.0×10^5 cells per well to generate a monolayer. After 18 h, the monolayer was infected with wild-type *L. monocytogenes* at an MOI of 0.01 in RPMI-1640. At 30 min post-infection, cells were washed three times with PBS and cultured in RPMI-1640 medium containing 10% FBS. At 60 min post-infection, cells were washed three times with PBS and RPMI-1640 containing 10% FBS, 10% L929 conditioned medium, and 50 μg ml^{-1} gentamycin was added to the cultures. At 18 h post-infection, cells were fixed with 2.5% PFA for 30 min at 37 °C and prepared for fluorescence microscopy. The number of infected cells per focus of infection was quantified using epifluorescence microscopy. Images for analysis were taken with a Hamamatsu Orca R2 camera and Nikon Ti-E microscope with ×10 objective and Volocity software (Improvision).

Live cell imaging of *L. monocytogenes* cell-to-cell spread. BMDMs were plated as a monolayer at 4×10^6 cells per well onto coverslips in a 6-well tissue culture plate. After 24 h, the monolayer was infected with *L. monocytogenes* expressing RFP (DP-L5538) at an MOI of 0.01 for 1 h. Cells were washed three times with PBS and incubated at 37 °C in RPMI containing 10% FBS, 10% L-929 conditioned medium and 50 μg ml^{-1} gentamycin. At 6 h post-infection, the coverslips were imaged in 25 mM HEPES buffered RPMI containing 10% FBS and 50 μg ml^{-1} gentamycin using a Quorum spinning disk confocal microscope (Leica DMIRE2 inverted fluorescence microscope equipped with a Hamamatsu back-thinned electron multiplying charge-coupled device camera, Yokogawa spinning disc head, and Volocity

6 software). Coverslips with BMDMs from control and *Timd4*$^{-/-}$ mice were placed side by side on a dual-chamber heated stage at 37 °C. Over the course of 12 h, 36 μm z stacks with a 2 μm step were taken every 15 min at ten foci of infection per coverslip. The channels for DIC and red fluorescence were acquired throughout the experiment. Image analysis was performed to measure the number of infected cells per infection focus during the course of the experiment.

Cell-to-cell spread assay. BMDMs from C57BL/6 mice were seeded at a density of 1×10^6 in 10 cm^2 Petri dishes 16 h before experiments. Cultures of Δ*plcA* Δ*plcB* mutant bacteria were used to infect BMDMs at an MOI of 10. At 60 min post-infection, cells were washed three times with PBS and RPMI medium containing 10% FBS and 50 μg ml^{-1} gentamycin was added to the cultures. At 3 h post-infection, cells were detached using CellStripper (Mediatech) containing 50 μg ml^{-1} gentamycin and counted. 1×10^5 infected cells were then overlaid onto fresh cultures of CellTracker Blue-labelled BMDMs from C57BL/6 or *Timd4*$^{-/-}$ mice. At 90 min after overlay, cells were fixed with 2.5% PFA for 30 min at 37 °C and prepared for fluorescence microscopy. The uptake of bacteria from infected primary cells (unlabelled) to secondary cells (CellTracker Blue labelled) was determined by microscopic analysis.

Labelling of secondary host cells with CellTracker Blue (Invitrogen) was performed as follows. Secondary cells were plated onto coverslips in 24-well tissue culture plates at 1.5×10^6 cells per well. At 2 h before overlay, serum-free RPMI medium containing 20 μM CellTracker Blue was added to the culture. After 30 min incubation, cells were washed three times with PBS and RPMI medium containing 10% FBS was added.

Macrophage replication assay. BMDMs were plated at 3×10^5 cells per well in 24-well tissue culture plates 24 h before infection. Cells were then infected with *L. monocytogenes* at an MOI of 1 in RPMI-1640. After 30 min of invasion at 37 °C, cells were washed three times with PBS followed by the addition of RPMI-1640. At 60 min post-infection, media was changed, and RPMI-1640 with 10% FBS containing 50 μg ml^{-1} gentamicin and 10% L929 was added. Cells were then lysed at 2, 4, 6, 8, 10 and 12 h post-infection with 1% Triton X-100 in PBS. Serial dilutions of the lysates were plated on BHI-agar plates and incubated at 37 °C for 16 h for subsequent quantification of intracellular c.f.u.

Mouse infection and tissue collection. Mice were infected with 5×10^4 c.f.u. wild-type or 1×10^7 c.f.u. Δ*actA* mutant *L. monocytogenes* (in 200 μl of PBS) via intravenous injection in the lateral tail vein. Liver and spleen were collected at 72 h post-infection. Organs were placed in 1 ml of sterile PBS and homogenized. A dilution series was plated on BHI plates, grown overnight at 37 °C and individual bacterial colonies were enumerated.

For cytokine analysis, cell culture supernatants and tissue homogenates were centrifuged (12,000 r.p.m. for 12 min) and supernatants were collected and stored at −80 °C. Cytokines were measured using the mouse 7-plex pro-inflammatory kit from Meso Scale Discovery, according to the manufacturer's instructions.

Statistical analysis. Statistical analyses were conducted using GraphPad Prism v.4.0a. The average ± s.d. is shown in figures, and *P* values were calculated as described in figure legends. A *P* value of less than 0.05 was considered statistically significant.

31. Bishop, D. K. & Hinrichs, D. J. Adoptive transfer of immunity to *Listeria monocytogenes*. The influence of *in vitro* stimulation on lymphocyte subset requirements. *J. Immunol.* **139,** 2005–2009 (1987).
32. Jones, S. & Portnoy, D. A. Characterization of *Listeria monocytogenes* pathogenesis in a strain expressing perfringolysin O in place of listeriolysin O. *Infect. Immun.* **62,** 5608–5613 (1994).
33. Lauer, P., Chow, M. Y., Loessner, M. J., Portnoy, D. A. & Calendar, R. Construction, characterization, and use of two *Listeria monocytogenes* site-specific phage integration vectors. *J. Bacteriol.* **184,** 4177–4186 (2002).
34. Skoble, J., Portnoy, D. A. & Welch, M. D. Three regions within ActA promote Arp2/3 complex-mediated actin nucleation and *Listeria monocytogenes* motility. *J. Cell Biol.* **150,** 527–538 (2000).
35. Smith, G. A. *et al.* The two distinct phospholipases C of *Listeria monocytogenes* have overlapping roles in escape from a vacuole and cell-to-cell spread. *Infect. Immun.* **63,** 4231–4237 (1995).
36. Shen, A. & Higgins, D. E. The 5′ untranslated region-mediated enhancement of intracellular listeriolysin O production is required for *Listeria monocytogenes* pathogenicity. *Mol. Microbiol.* **57,** 1460–1473 (2005).
37. Rodriguez-Manzanet, R. *et al.* TIM-4 expressed on APCs induces T cell expansion and survival. *J. Immunol.* **180,** 4706–4713 (2008).
38. Munsie, L. N., Caron, N., Desmond, C. R. & Truant, R. Lifeact cannot visualize some forms of stress-induced twisted F-actin. *Nature Methods* **6,** 317 (2009).
39. Brumell, J. H., Rosenberger, C. M., Gotto, G. T., Marcus, S. L. & Finlay, B. B. SifA permits survival and replication of *Salmonella typhimurium* in murine macrophages. *Cell. Microbiol.* **3,** 75–84 (2001).

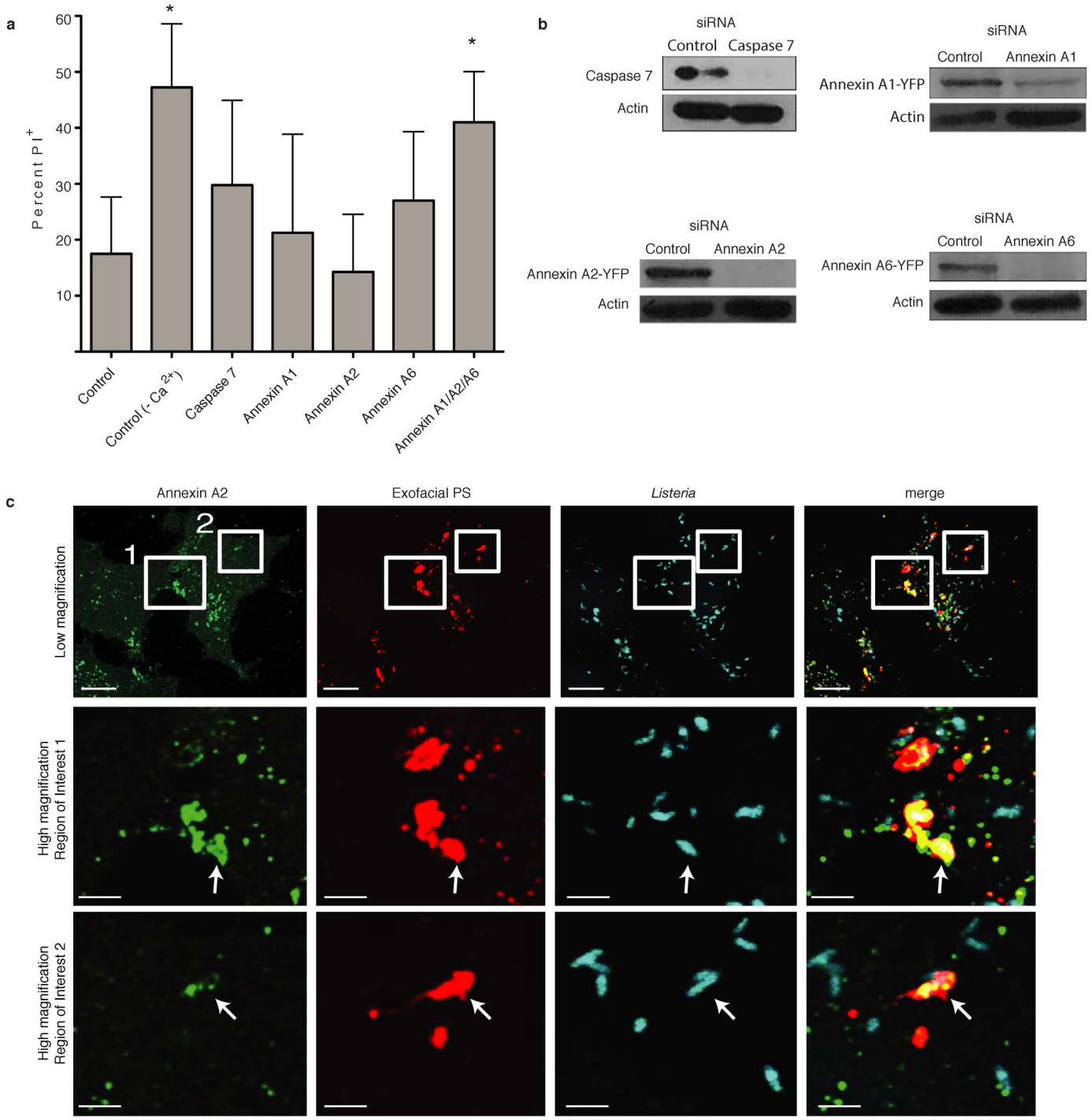

Extended Data Figure 1 | Annexins promote membrane repair during *L. monocytogenes* infection. **a**, HeLa cells were treated with the indicated siRNA for 48 h and then infected with wild-type *L. monocytogenes* at an MOI of 100. At 6 h post-infection, medium was switched to Tyrodes buffer containing 0.5 mg ml^{-1} PI with or without calcium. Cells were fixed at 60 min after PI addition and then stained for bacteria and DNA (DAPI). The percentage of 100 random infected cells that were PI^{+} cells were enumerated by microscopic analysis. Averages ± s.d. for three independent experiments are shown. *P* values were calculated using one-way ANOVA. *$P < 0.05$. **b**, Knockdown of gene expression by siRNA was confirmed by western blotting. Images are representative of two independent experiments. **c**, Recruitment of annexin A2 to PS^{+} structures containing bacteria. Boxes in low-magnification image indicate areas enlarged in bottom panels. Arrows indicate PS^{+} structures that co-localize with annexin A2. Images are representative of three independent experiments. Scale bars, 10 µm for low-magnification images, 2 µm for enlarged regions of interest.

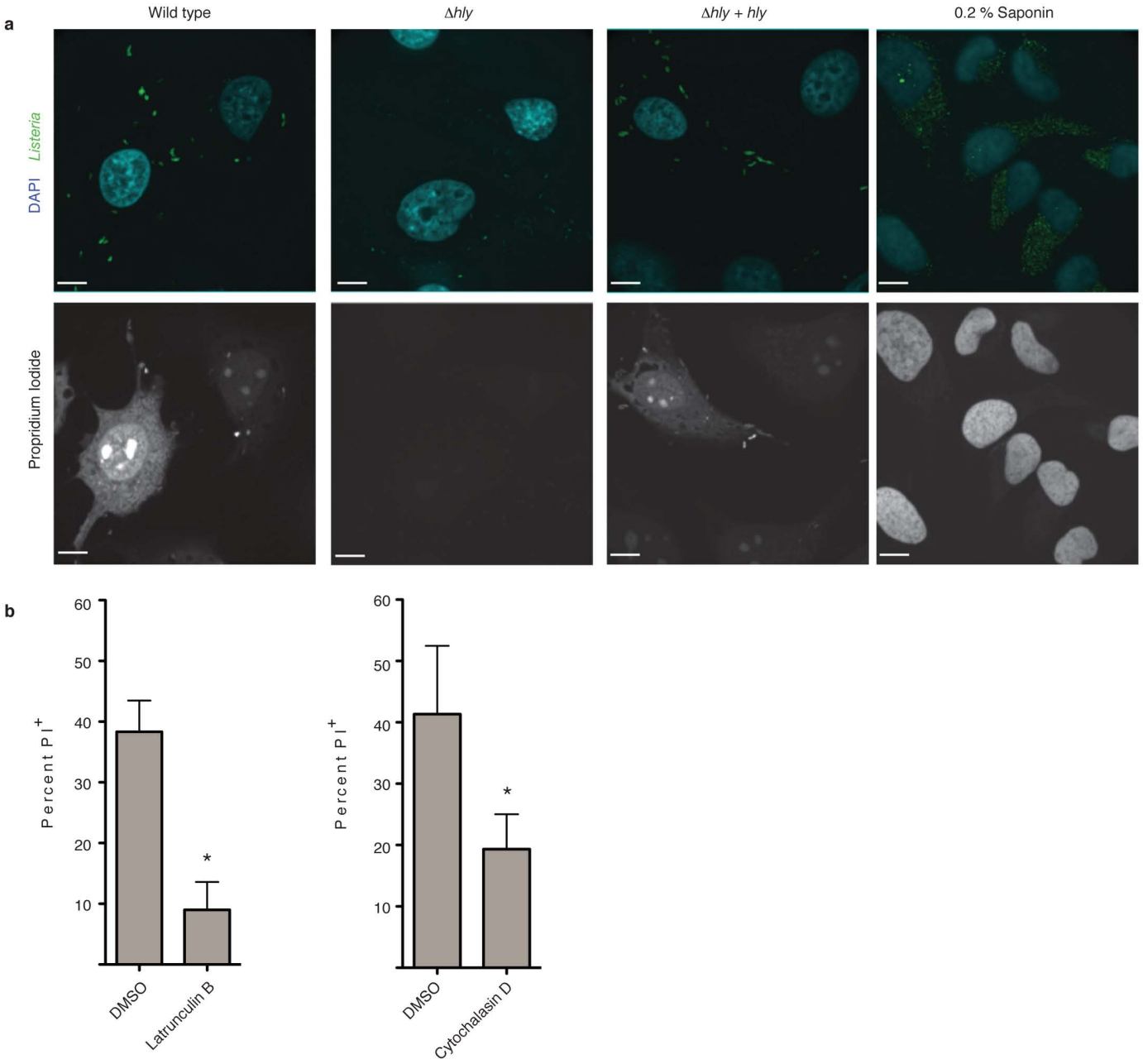

Extended Data Figure 2 | Actin-based motility promotes LLO-mediated membrane damage during *L. monocytogenes* infection. **a**, HeLa cells were infected with the indicated *L. monocytogenes* strain. At 6 h post-infection, medium was switched to Tyrodes buffer containing 0.5 mg ml^{-1} PI with or without calcium. Cells were fixed at 60 min after PI addition and then stained for bacteria and DNA (DAPI). Confocal images representative of three independent experiments are shown ($n = 100$). PI^{+} cells were enumerated and results are shown in Fig. 1d. Where indicated, uninfected cells were treated with saponin to permeabilize membranes and allow PI entry, serving as a positive control. Scale bars, 10 μm. **b,** HeLa cells were infected with wild-type *L. monocytogenes* and subjected to membrane damage assay as in **a** in the presence of either DMSO or the actin cytoskeleton inhibitors latrunculin B or cytochalasin D. Averages ± s.d. for three independent experiments are shown ($n = 100$). *P* values were calculated using two-tailed Student's *t*-test. *$P < 0.05$.

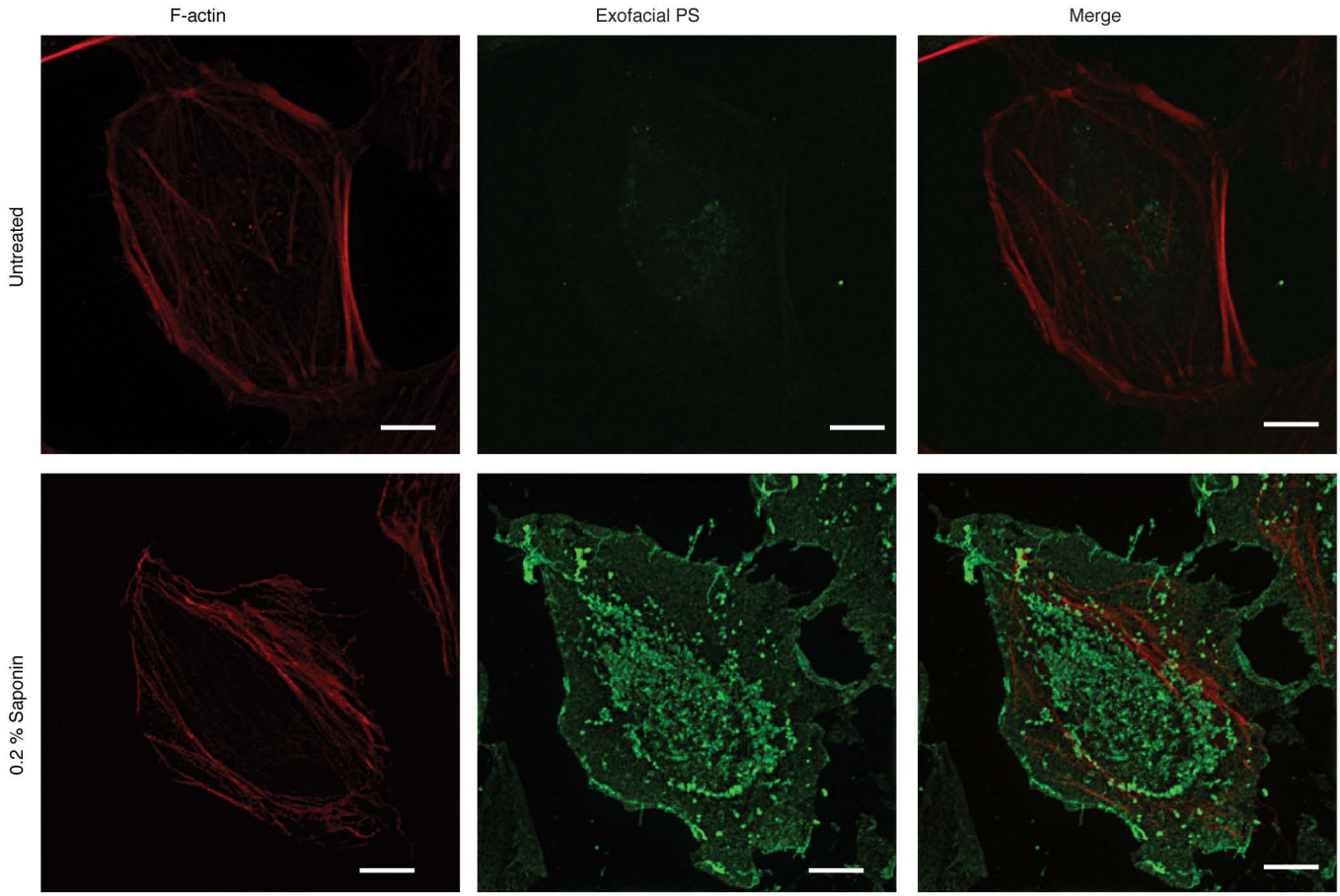

Extended Data Figure 3 | Annexin A5–Alexa 488 as a probe to label PS. Live HeLa cells were cooled on ice and stained with a fluorescent probe (annexin A5–Alexa 488) for 10 min to label exofacial PS. Cells were then fixed and stained with phalloidin Alexa 568 to visualize F-actin. In uninfected control experiments, low amounts of exofacial PS was detected in the membranes of cells, due to asymmetry of PS distribution in the plasma membrane. By contrast, treatment of cells with the pore-forming surfactant saponin led to robust staining of cells with annexin A5–Alexa 488. Images representative of three independent experiments. Scale bars, 10 μm.

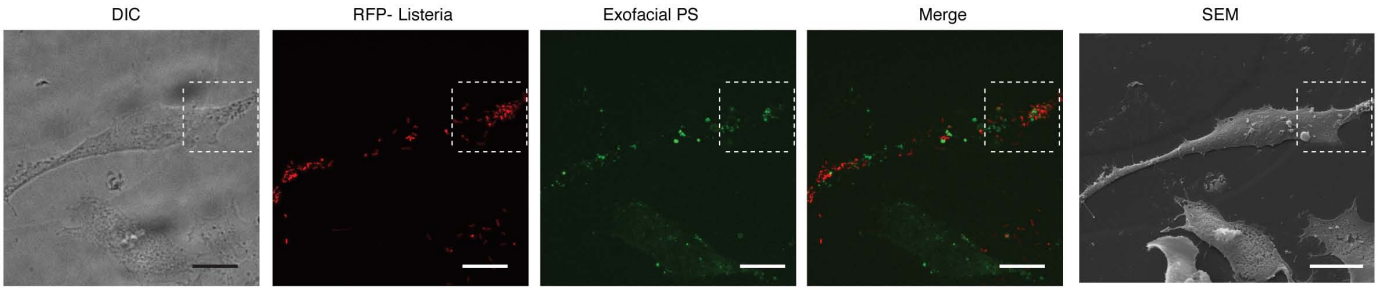

Extended Data Figure 4 | Formation of PS^+ structures during *L. monocytogenes* infection. Low-magnification images used to generate images shown in Fig. 2a. HeLa cells were infected with wild-type *L. monocytogenes* expressing RFP for 6 h and then cooled on ice and stained with a fluorescent probe (annexin A5–Alexa 488) for 10 min to label exofacial PS. Cells were then fixed and analysed by fluorescence microscopy to identify PS^+ structures and bacteria. SEM of the same cell revealed that PS^+ structures were associated with the dorsal surface of infected cells. Differential interference contrast (DIC) microscopy of cells was also performed to help identify cells for correlative imaging analysis. Images are representative of two independent experiments. Scale bars, 20 μm.

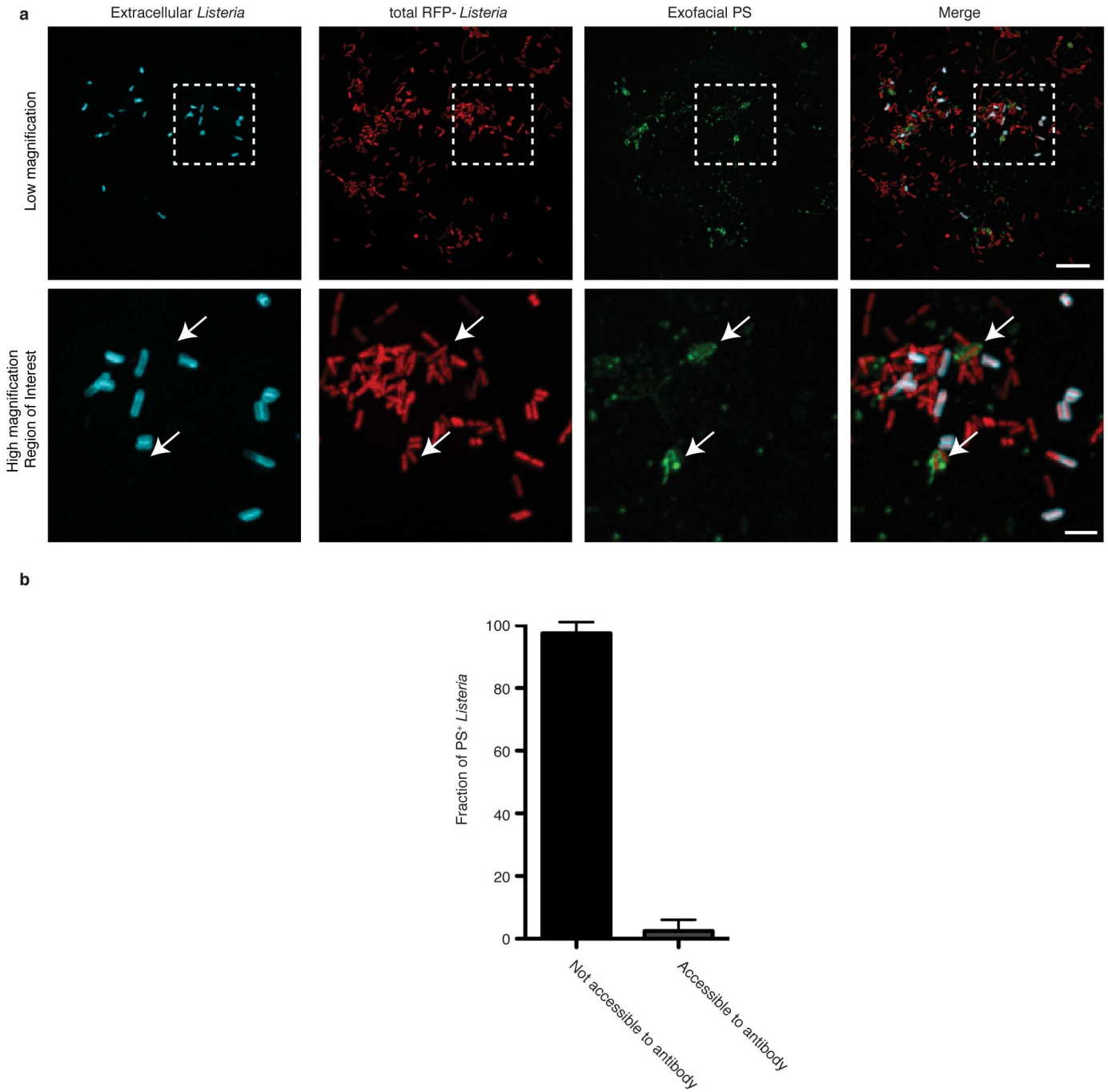

Extended Data Figure 5 | PS$^+$ bacteria are present with a host-derived membrane structure. **a**, HeLa cells were infected with wild-type *L. monocytogenes* expressing RFP for 8 h and then labelled with a probe for exofacial PS (annexin A5–Alexa 488). Cells were then rapidly stained with anti-*Listeria* antibodies (5 min) to label extracellular bacteria. Cells were then fixed and analysed by fluorescence microscopy to identify PS$^+$ structures and bacteria. Bacteria that co-localize with exofacial PS but are not labelled with anti-*Listeria* antibodies in the extracellular medium are indicated with arrows. Extracellular bacteria do not label with annexin A5–Alexa 488, indicating that this probe does not bind non-specifically to bacteria. Box in low-magnification image indicates area enlarged in bottom panels. Images are representative of three independent experiments. Scale bars, 10 μm for low magnification, 2 μm for high magnification. **b**, Cells were infected and stained as in **a** and analysed by fluorescence microscopy. Bacteria that co-localize with exofacial PS were scored for their accessibility to anti-*Listeria* antibodies present in the extracellular medium. Data show that the majority of PS$^+$ bacteria are not accessible to anti-*Listeria* antibodies. Averages ± s.d. for two independent experiments are shown ($n = 100$).

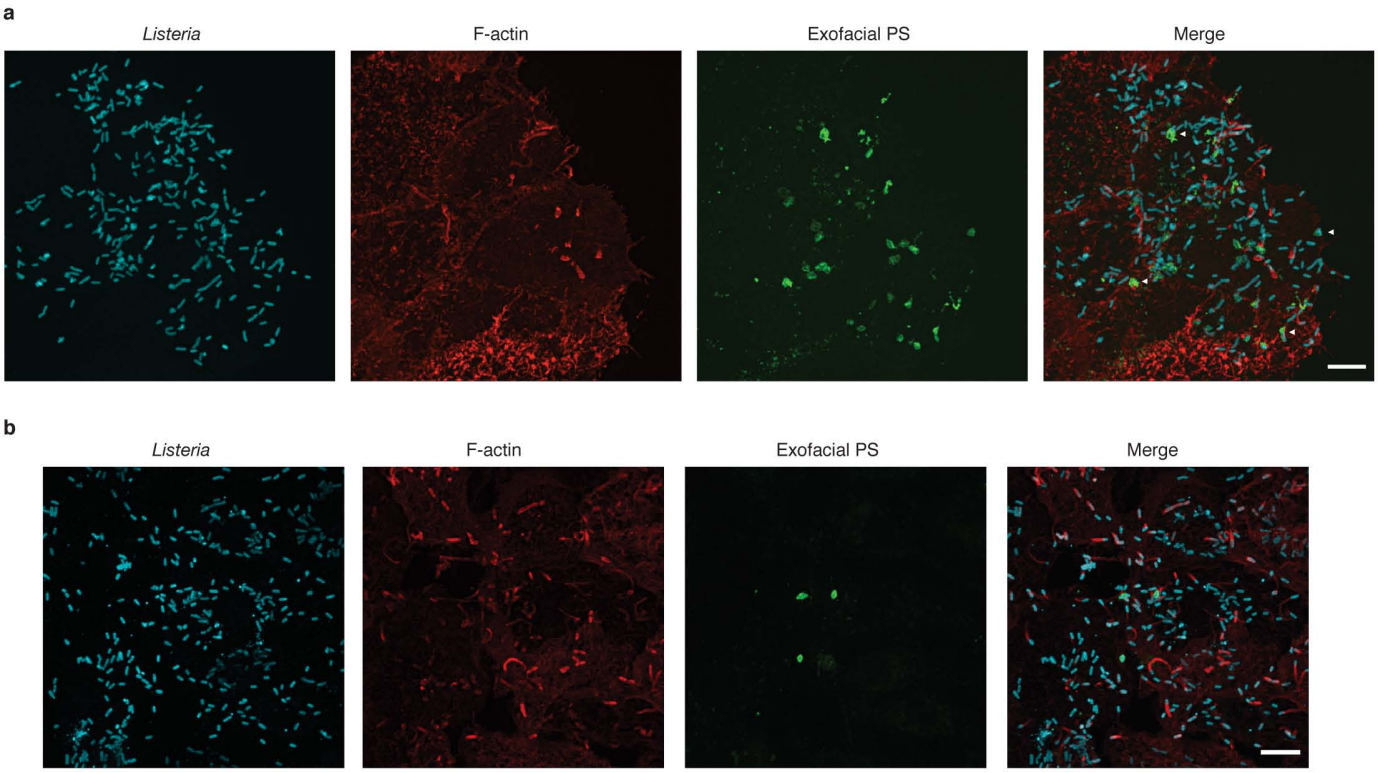

Extended Data Figure 6 | Formation of PS^+ structures during *L. monocytogenes* infection of epithelial cells and macrophages. **a**, Henle-407 human intestinal epithelial cells were infected with wild-type *L. monocytogenes* for 6 h and then incubated with a probe for exofacial PS (annexin A5–Alexa 488; green). Cells were then fixed and stained with phalloidin to visualize F-actin (red) and bacteria (blue). Cells were analysed by fluorescence microscopy to identify PS^+ structures and bacteria. Images are representative of three independent experiments. **b**, Mouse BMDMs from C57BL/6 mice were infected and stained as in **a**. Scale bars, 10 μm. Images are representative of three independent experiments.

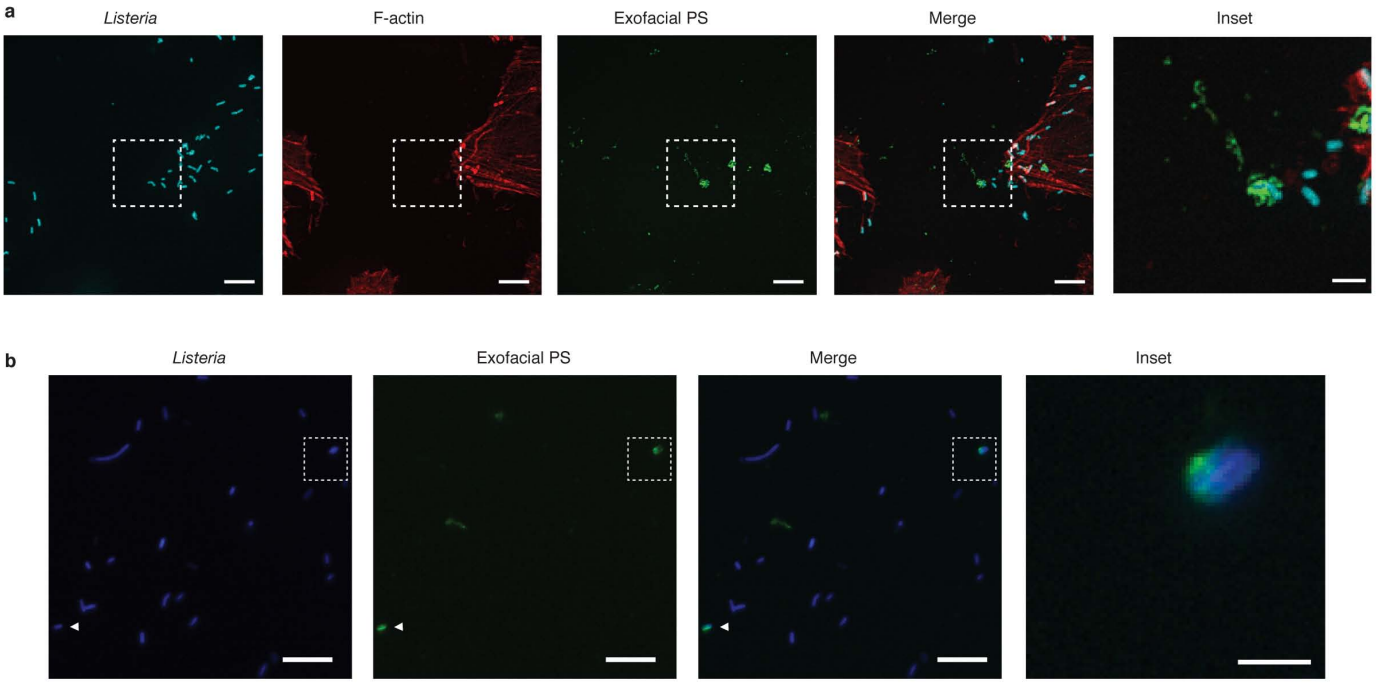

Extended Data Figure 7 | Release of PS$^+$ structures containing *L. monocytogenes* from infected cells. **a**, HeLa cells were infected with wild-type *L. monocytogenes* for 6 h and then incubated with a probe for exofacial PS (annexin A5–Alexa 488; green). Cells were then fixed and stained with phalloidin to visualize F-actin (red) and bacteria (blue). Cells were analysed by fluorescence microscopy to identify PS$^+$ structures and bacteria. Inset shows PS$^+$ bacteria that are not cell associated. Images are representative of three independent experiments. **b**, HeLa cells were infected with Δ*plcA*Δ*plcB* mutant bacteria for 6 h. The supernatant from the infected cultures was then removed and centrifuged onto poly-L-lysine-coated coverslips. Bacteria associated with coverslips were then stained with a probe for exofacial PS (annexin A5–Alexa 488; green). Cells were then fixed and stained for bacteria (blue). Coverslips were analysed by fluorescence microscopy to identify PS$^+$ bacteria. Inset shows PS$^+$ bacteria. Scale bars, 10 μm for low-magnification images, 2 μm for insets. Images are representative of three independent experiments.

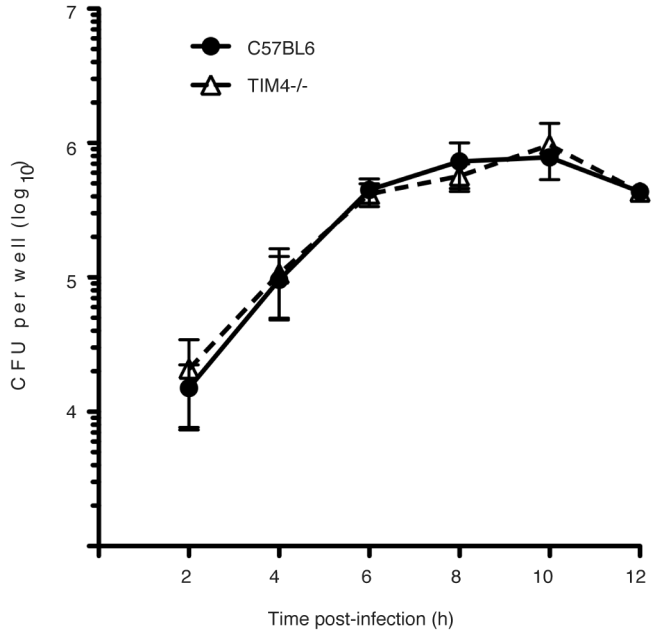

Extended Data Figure 8 | Growth of *L. monocytogenes* in the cytosol of *Timd4*$^{-/-}$ macrophages is not impaired. Gentamicin protection assay to measure intracellular bacterial growth. BMDMs were harvested from C57BL/6 or *Timd4*$^{-/-}$ mice and seeded at a density of 3×10^5 cells per well. Cells were then infected with wild-type *L. monocytogenes* in the presence of extracellular gentamicin. At the indicated times, cell lysates were plated and intracellular bacterial numbers (c.f.u.) were determined. Averages ± s.d. for two independent experiments are shown.

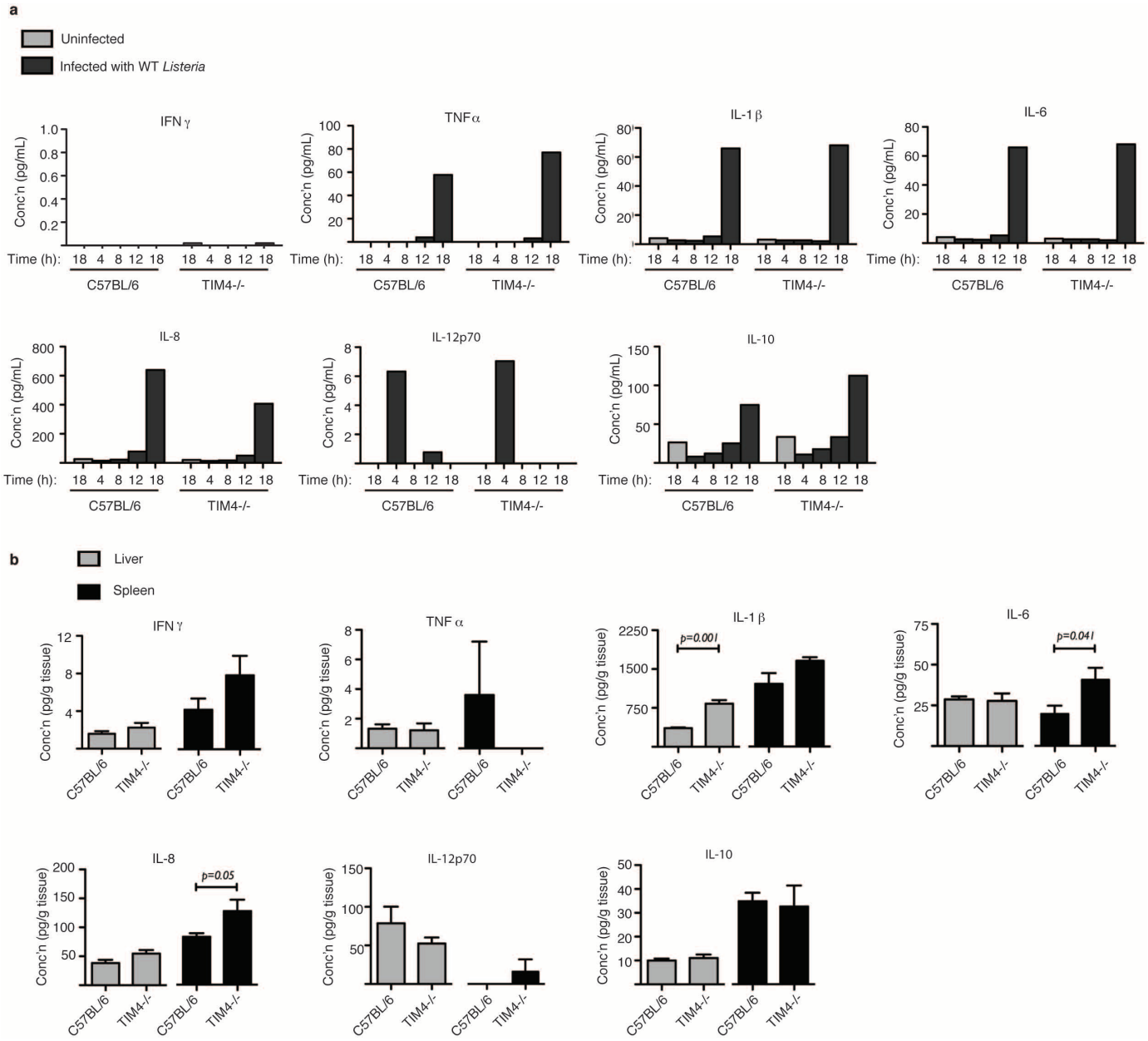

Extended Data Figure 9 | Cytokine measurements. **a**, Measurement of cytokines after *in vitro* infection of BMDMs from C57BL/6 or *Timd4*$^{-/-}$ mice with wild-type *L. monocytogenes* for the indicated time. Data from one of two independent experiments are shown. **b**, Measurement of basal cytokines in tissues of C57BL/6 or *Timd4*$^{-/-}$ mice without infection. Averages ± s.d. for three independent experiments are shown. *P* values were calculated using one-way ANOVA.

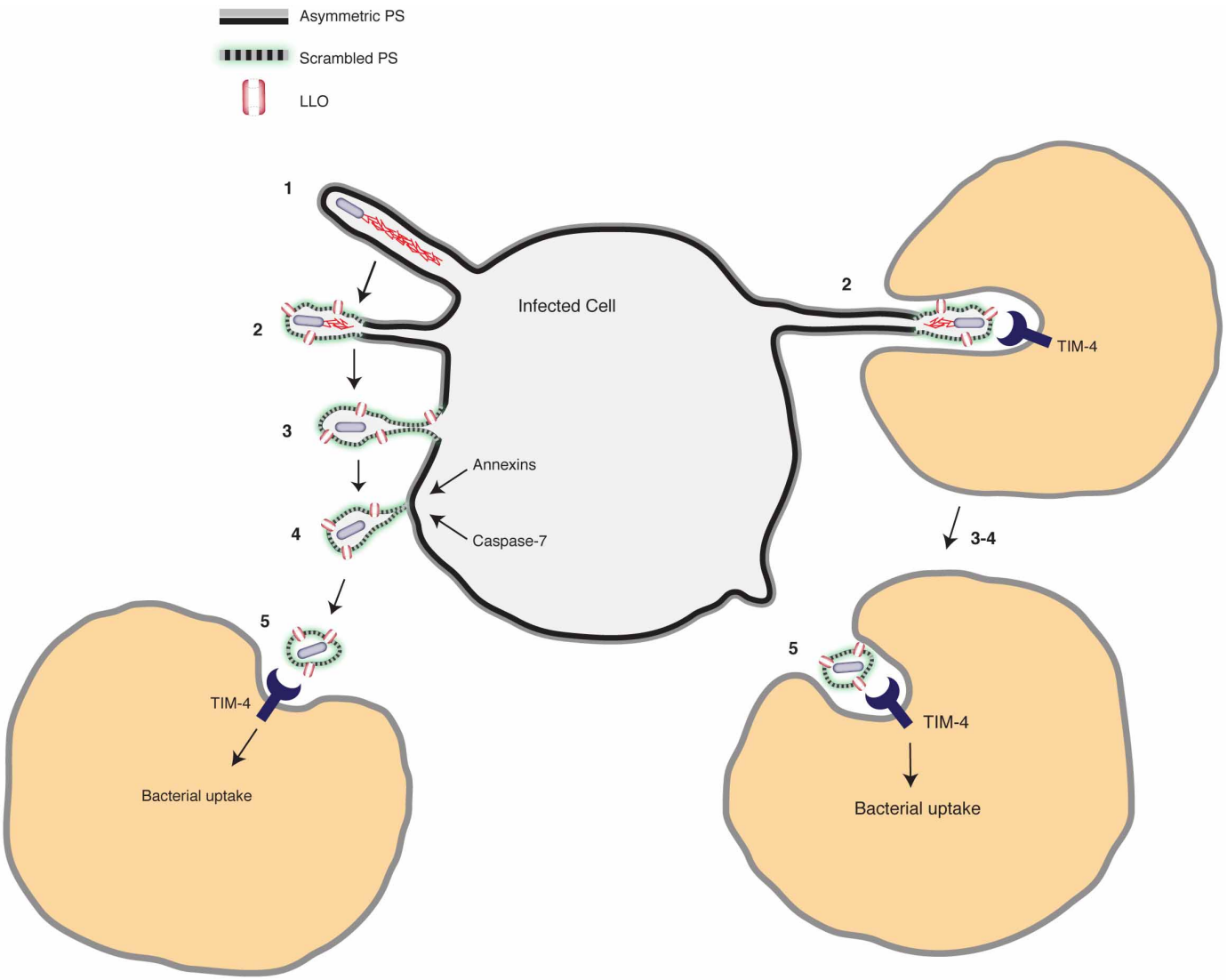

Extended Data Figure 10 | *L. monocytogenes* exploits efferocytosis to promote cell-to-cell spread during infection. Model shows the steps that promote cell-to-cell spread by *L. monocytogenes*. **1.** Protrusion formation via actin-based motility. **2.** LLO-mediated damage to the plasma membrane leads to loss of membrane asymmetry and exofacial PS on protrusions. The exofacial exposure of PS promotes protrusion association with neighbouring cells (right). **3.** Loss of membrane asymmetry and PS exposure extends along length of protrusions. **4.** Calcium entry activates membrane repair pathways that promote scission of the protrusion. Bacteria are released from the cell in PS^+ vesicles. **5.** Macrophages mediate uptake of PS^+ vesicles containing bacteria via the PS-binding receptor TIM-4. PS^+ vesicles may be engulfed by neighbouring cells either near the infected cell surface (left side) or within enclosed spaces that form as a result of protrusion penetration into the neighbouring cell (right side). TIM-4 may also promote *L. monocytogenes* infection indirectly, through its ability to suppress basal levels of pro-inflammatory cytokines as part of its homeostatic function in the immune system.